CASL-U-2015-0116-000

Implementation and Preliminary Verification of the Quasi-1D Kernel for Intra-pin Resonance Physics in MPACT

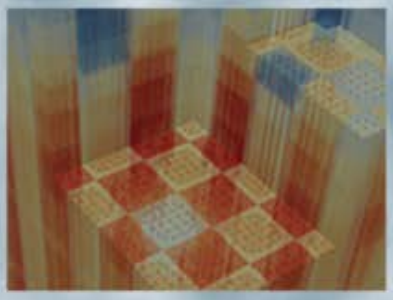

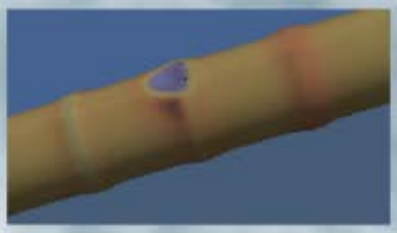

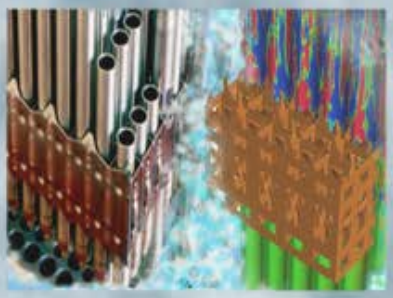

Yuxuan Liu and William Martin
University of Michigan

March 16, 2015

U.S. DEPARTMENT OF ENERGY | Nuclear Energy

CASL-U-2015-0116-000

Implementation and Preliminary Verification of the Quasi-1D Kernel for Intra-pin Resonance Physics in MPACT

Yuxuan Liu and William Martin

University of Michigan

L3:RTM.SUP.P10.03 Milestone Report

March 16, 2015

CASL-U-2015-0116-000

EXECUTIVE SUMMARY

A new resonance self-shielding method ESSM-X has been developed as part of the first author's PhD dissertation in order to model the within-pin resonance self-shielding physics with improved accuracy. The method performs the conventional ESSM without subdivision of the fuel region to capture the inter-pin shielding effect. The resultant self-shielded cross sections are modified by correction factors incorporating the intra-pin effects of radial variation of the shielded cross section (distributed self-shielding), radial temperature distribution and resonance interference. These correction factors are computed through an efficient quasi-1D slowing-down model. The method has been incorporated into the DeCART transport code and the results show that the new method yields substantially improved results for both radially dependent and energy-dependent reaction rates, which help to improve the within-pin physics for multi-region depletion and multiphysics calculations, as well as the overall eigenvalue estimation.

This report describes the implementation of ESSM-X into MPACT and its preliminary assessment using a set of 2-D infinite pin cell problems. The results show significant improvement of ESSM-X in treating the within-pin resonance physics, as compared to the conventional ESSM and the subgroup method. The additional computing time of the new method is small due to the high efficiency of the quasi-1D model and the additional memory needed by the method does not increase with the geometrical size of the problem.

1. Introduction

Evaluation of effective multigroup cross sections is a crucial topic for deterministic neutron transport calculation. For this task, the resonance self-shielding methods based on integral table interpolation shows much better efficiency than directly solving the continuous energy (CE) slowing-down equation of the problem of interest. However the derivation of integral table based methods introduces a number of approximations leading to issues in modeling resonance interference, distributed self-shielding (multiple fuel regions) and non-uniform temperature profiles within the fuel rod.

A new resonance self-shielding model ESSM-X has been developed to account for the three important effects. It is a fusion of two types of methods, the integral table method and the direct slowing-down method. The assumption that underpins this new method is that the global Dancoff effect is treated satisfactorily with ESSM, while the effects of radial fuel regions, resonance interference, and non-uniform temperatures are local phenomena that can be treated with a continuous energy slowing-down equation for the local geometry. Thus conventional ESSM is still performed for every 2-D plane of the problem as a baseline calculation to capture the global resonance (Dancoff) effects. Complementing this, the new method introduces a 1-D model to explicitly account for the intra-pin (local) effects. To connect the local 1-D fuel pin calculation with the global ESSM calculation, a quasi-1D form of the slowing-down equation is developed that incorporates an equivalence cross section that accounts for the boundary conditions implicitly, rather than using explicit boundary conditions, hence ‘quasi-1D’. In addition, effort has been made to improve the efficiency of the quasi-1D slowing-down solver. Finally, a correction procedure is designed to modify the effective cross section obtained from ESSM by using correction factors calculated from the quasi-1D model to account for radial shielding, non-uniform temperature effects, and resonance interference.

ESSM-X had been implemented in DeCART transport code and the results showed that the within-pin physics related to the self-shielding calculation were significantly improved by ESSM-X. The detailed description of the method can be found in Ref. [1]. This document primarily focuses on the recent implementation of ESSM-X in MPACT. A set of 2-D pin cell cases which were used to test the ESSM-X in DeCART are reused to show the consistent performance of ESSM-X in MPACT. The computational resources of ESSM-X are also investigated.

2. Method Implementation

The first step of ESSM-X is to perform the regular ESSM to account for the 2-D whole-core Dancoff effect. The quantities obtained by the first step include the equivalence cross sections of resonant fuel regions as well as the base effective cross sections for each isotope of a fuel rod (no subdivision). Since ESSM capability has already been incorporated into MPACT, this step requires no extra work.

The second step of ESSM-X involves the calculation of two sets of effective cross sections in order to obtain the resonance correction factors

$$f_{iso,x,g,i} = \frac{\sigma_{iso,x,g,i}}{\sigma_{iso,x,g,F}} \tag{1}$$

In this equation, $f_{iso,x,g,i}$ is defined for isotope *iso*, reaction channel *x*, energy group *g* and fuel subregion *i*. The effective cross sections of both sets are obtained using the neutron spectra computed by quasi-1D slowing-down model. The numerator $\sigma_{iso,x,g,i}$ is for a resonance isotope in subregion *i* with realistic number density and temperature as well as the presence of other resonance isotopes (interference effect), however, the denominator $\sigma_{iso,x,g,F}$ is for an isolated isotope with averaged density and temperature over the whole fuel region (conditions similar to the first step). The following subsections discuss the calculation of $\sigma_{iso,x,g,i}$ and $\sigma_{iso,x,g,F}$.

2.1 Calculation of $\sigma_{iso,x,g,i}$

The quasi-1D slowing-down equation is solved on the fly in order to obtain $\sigma_{iso,x,g,i}$. The functionalities implemented to support the quasi-1D calculation include:

1. A reader to process AMPX continuous-energy (CE) library. Specifically, the total cross section and elastic scattering cross section are needed to solve the slowing-down equation. Fission cross section for fissionable isotopes is also read in to compute the correction factors.
2. The quasi-1D slowing-down kernel. To compute the collision probability for 1-D cylindrical geometry, Carlvik's method [2] is incorporated into the module.
3. Supporting functions to determine the energy mesh scheme of slowing-down solver.
4. Cross section manipulation (interpolation, collapsing, etc.)

For # 3, two energy mesh schemes could be options, the equal lethargy mesh and the problem dependent mesh. Currently the problem dependent mesh has been implemented in MPACT since it is more efficient in solving heterogeneous slowing-down problems (fewer fixed source problems due to smaller number of meshes). The unionized problem-dependent mesh is determined as follows:

a. Scan the problem of the geometrically decomposed domain and record all isotopes in the fuel regions.
b. Read the cross section data of these isotopes from the AMPX CE library at several discrete temperatures according to the library availability (say 296K, 600K, 900K, 1200K and 2400K).
c. Map the cross section of each isotope to the energy mesh of the lowest temperature (say 296K) so that every isotope ends up with a uniform energy mesh of cross sections for different temperatures.
d. Generate a union mesh for each fuel material composition using an approach similar to CENTRM [3]. The energy meshes of isotopes in a material are unionized and thinned in such a manner that the macroscopic total cross section can be linearly interpolated according to a specific tolerance.
e. Combine the energy meshes of all fuel materials in the problem domain to a final union mesh 'M' (this will be used for the slowing-down calculation). Alternatively, the energy meshes of fuel materials in each pin are combined separately, so pin *i* can have an independent union mesh 'M_i'. The former is better for fresh fuel case where the number of different materials (composition & temperature) is relatively small, while the latter is better for depleted case or case with thermal feedback where the number of different materials is large. User options are available in MPACT to use M or M_i.
f. During the slowing-down calculation, interpolation is needed to obtain the cross section at a specific temperature on the union mesh 'M' or 'M_i'. In order to save memory, the isotopic cross section is only stored under its own energy mesh. The cross section at a union mesh point is interpolated as needed in the slowing-down calculation. An indexing array for each isotope is pre-computed to facilitate the interpolation.
g. When collapsing the MG cross section of an isotope using point-wise spectrum from quasi-1D slowing-down calculation, the union mesh 'M' or 'M_i' is combined with the cross section energy mesh of the isotope in order to retrieve the subtleties of cross section variation versus energy for the isotope (these subtleties might have been lost during mesh thinning).

2.2 Calculation of $\sigma_{iso,x,g,F}$

Instead of solving the quasi-1D slowing-down equation on the fly to obtain the denominator $\sigma_{iso,x,g,F}$ of Equation (1), a second set of RI tables has been introduced for interpolation of $\sigma_{iso,x,g,F}$. Suppose there are *n* resonance isotopes in a fuel pin, without using the second set of RI tables, the quasi-1D slowing-down calculation should be performed *n*+1 times (n times for the isolated resonance isotopes and one more time for the mixture). By using the second set of RI tables, the computing time for quasi-1D slowing-down is significantly reduced, especially for the complex fuel compositions such as MOX or burned fuels.

Given the conditions of computing $\sigma_{iso,x,g,F}$ is similar to the base case of ESSM in the first step, the only difference using the new RI tables compared to the standard RI tables (for ESSM calculation) is that the new tables utilize the quasi-1D solver for slowing-down calculation. In terms of consistency, both sets of RI tables should be generated using the same point-wise cross section data source and same fixed source solver to establish the correlation of RI versus background cross section. A temporary solution for the present verifications is to generate these two sets of tables using UM developed slowing-down and fixed source solvers, as shown in Figure 1. These RI tables are generated upon the 56-group ORNL library structure, thus should be utilized together with other non-resonance data of the 56-group library. *In the long run, these data should be consistently generated through the AMPX cross section processing system with the Multigroup library being used in CASL.*

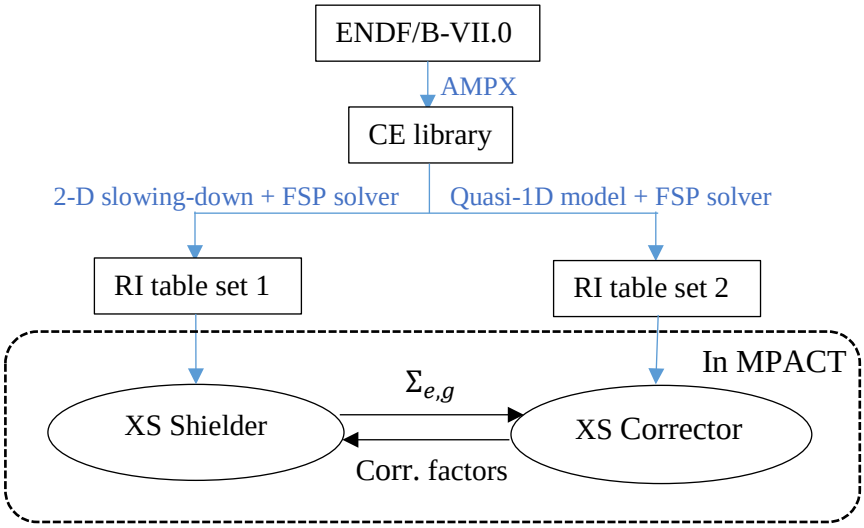

Figure 1 Data flow of the Quasi-1D resonance model

3. Numerical Results

A set of 2-D infinite pin cell problems have been tested to compare the capability of the resonance methods for treating distributed self-shielding, resonance interference and non-uniform temperature effects. These cases are adapted from VERA Core Physics Benchmark Problems [4] with modifications such as temperature distribution and material composition in order to test these effects.

Table 1 Description of test problems

#	Case ID	Description
1	UO2_600K	5% UO2 pin cell with uniform fuel Temp. of 600K
2	UO2_900K	5% UO2 pin cell with uniform fuel Temp. of 900K
3	UO2_1200K	5% UO2 pin cell with uniform fuel Temp. of 1200K
4	UO2_para900K	5% UO2 pin cell with parabolic fuel Temp. - Ave. 900K
5	UO2_para1200K	5% UO2 pin cell with parabolic fuel Temp. - Ave. 1200K
6	UO2_3%	3% UO2 pin cell
7	UO2_4%	4% UO2 pin cell
8	UO2_Gd	Gadolinium integrated UO2 fuel
9	MOX_16%	MOX fuel with 16% Plutonium

The test problems are run by the subgroup method, ESSM and ESSM-X of MPACT with the ORNL 56-group library (ESSM-X replace the RI tables with those described in the previous section). The fuel rod is subdivided into 10 equal-volume rings. The same MOC ray options (Chebyshev-Bickley with 4 polar angles, 24 azimuthal angles in 90° and 0.01cm ray spacing) are applied to all the test problems. The ESSM and the subgroup method use Bondarenko iteration for treatment of resonance interference. The adjustment method for treating the non-uniform temperature distribution [5] in the subgroup method has also been toggled on. For each case, the MCNP reference solution is calculated with 600 active cycles and 50,000 histories/cycle to make a total of 30 million neutron histories. As a result, the standard deviation of reaction rates for every reaction channel and every resonance energy group is below 1%, and the standard deviations of reaction rates over the resonance energy range (0.625eV-25keV) for important resonance isotopes (U-235, U-238, Pu-239 and Pu-240) are on the order of 0.02%.

First we verify the effective cross section, which is a direct product of the resonance calculation. Table 2 compares the radially dependent shielded cross sections for U-238 in Group 34 (6.5eV-6.88eV) for the three methods with MCNP. Since this is the major resonance of U-238, strong spatial self-shielding is seen from the reference solution, e.g., the shielded cross section for the outermost ring is almost three times that for the innermost ring for Case 1. It is interesting to note that the shielded cross section of Group 34 is not monotonically increasing from the fuel center to the surface for the uniform temperature cases. The values become a bit larger towards the center for the innermost four or five rings. This can be explained by comparing the CE fluxes of every fuel ring,

in which the fluxes of the inner rings are relatively flatter about energy than those of the middle rings due to the strong spatial shielding. The relative errors show that ESSM is unable to correctly produce the spatially shielded cross sections. For all the nine cases, it underestimates the cross sections of the surface ring and overestimates those of the inner rings. Compared to ESSM, the subgroup method performs better for the surface ring, but still has large discrepancies for the inner rings. The shielded cross sections generated by ESSM-X compare favorably with MCNP results, showing an order of magnitude smaller relative error compared to the ESSM and subgroup method. The agreement of non-uniform temperature cases is on the same order as the agreement with the uniform temperature cases. The agreement of other resonance groups is similar to Group 34 and thus the results are not repeated.

Table 3 shows the spatially dependent absorption cross sections of U-235 for Group 22 (116.0eV-117.5eV) where the resonance interference due to U-238 is significant. Because the spectra are dominated by U-238 absorption resonances, the usual shielding behavior where the effective cross section tends to the peak at the fuel surface is not seen in this group for U-235. ESSM and the subgroup method using Bondarenko iteration fail to model the resonance interference, so large discrepancies are observed across all the rings of the fuel rod. It is clear from Table 3 that errors of shielded cross sections are reduced to less than 1% for most subregions with ESSM-X, indicating the success of employing CE cross sections explicitly for interference correction.

Table 2 Comparison of spatially shielded U-238 absorption cross sections for Group 34 (6.5eV-6.88eV) with MCNP showing effect of radial fuel subregions

Case		Ring number									
		1	2	3	4	5	6	7	8	9	10
1 (UO2_600K)	Ref. XS	415.1	407.3	390.2	380.5	376.0	374.0	386.0	423.0	541.3	1206.9
	Subgroup	28.5	30.2	35.0	37.1	36.9	35.1	27.9	14.9	-4.5	-16.4
	ESSM	46.7	50.9	57.7	61.7	64.8	69.9	67.7	57.3	29.2	-34.2
	ESSM-X	-2.9	-4.1	-2.6	-2.1	-2.0	-0.8	-0.4	-0.2	0.2	-1.9
2 (UO2_900K)	Ref. XS	688.9	662.8	634.0	606.2	578.1	565.9	566.8	610.9	769.4	1453.5
	Subgroup	22.6	27.0	32.0	36.6	40.7	39.7	34.2	20.2	-0.4	-10.2
	ESSM	30.2	35.6	42.3	49.5	56.5	60.7	64.8	56.4	27.9	-25.1
	ESSM-X	-3.0	-3.7	-3.9	-3.8	-2.7	-2.5	-1.4	-0.9	-0.1	-1.7
3 (UO2_1200K)	Ref. XS	1011.1	980.3	933.2	877.8	827.9	785.9	770.0	808.1	986.4	1616.6
	Subgroup	15.3	18.7	24.2	30.7	35.8	38.2	34.2	21.6	1.9	-5.9
	ESSM	15.4	19.0	25.2	33.5	41.6	49.1	54.0	49.9	25.1	-18.0
	ESSM-X	-3.2	-4.5	-4.7	-4.2	-3.9	-3.0	-2.1	-0.9	0.2	-1.4
4 (UO2_para900K)	Ref. XS	892.2	791.8	712.2	632.5	577.6	538.0	513.8	519.9	612.4	1250.8
	Subgroup	4.7	12.9	22.0	32.2	38.6	38.5	31.5	20.8	6.2	-6.8
	ESSM	5.08	13.54	23.70	36.38	46.80	54.37	58.21	52.27	26.51	-25.05
	ESSM-X	-5.83	-4.89	-4.30	-2.99	-2.99	-2.44	-1.79	-0.77	-0.15	-2.17
5 (UO2_para1200K)	Ref. XS	1200.9	1092.8	987.6	882.8	804.6	740.4	701.6	706.8	833.5	1481.8
	Subgroup	-8.4	2.1	14.0	27.7	38.5	46.4	46.7	37.3	17.3	-4.8
	ESSM	5.1	13.5	23.7	36.4	46.8	54.4	58.2	52.3	26.5	-24.9
	ESSM-X	-5.9	-4.9	-4.3	-3.0	-3.0	-2.5	-1.8	-0.8	-0.1	-2.1
6 (UO2_3%)	Ref. XS	421.5	401.9	391.7	381.4	375.7	376.1	386.1	421.7	538.0	1202.5
	Subgroup	26.3	31.7	34.2	36.6	36.9	34.2	27.7	15.0	-4.5	-16.6
	ESSM	42.20	50.39	56.86	61.23	64.28	67.50	67.00	57.34	29.36	-34.16
	ESSM-X	-3.87	-2.40	-2.65	-2.21	-1.89	-1.55	-0.84	-0.55	-0.22	-2.07
7 (UO2_4%)	Ref. XS	415.0	405.2	391.5	382.9	377.8	373.2	386.7	423.3	538.5	1209.0
	Subgroup	28.4	30.8	34.4	36.1	36.1	35.3	27.6	14.7	-4.3	-16.8
	ESSM	45.5	50.4	57.3	60.6	63.6	69.5	67.0	57.0	29.5	-34.4
	ESSM-X	-2.6	-3.4	-2.7	-2.7	-2.5	-0.7	-0.8	-0.6	0.2	-2.3
8 (UO2_Gd)	Ref. XS	402.5	389.5	379.7	371.4	375.6	375.4	393.4	434.8	567.3	1237.1
	Subgroup	31.3	34.8	37.2	38.8	35.3	32.9	24.3	11.8	-6.6	-16.3
	ESSM	52.9	57.9	62.1	66.6	67.4	71.0	67.4	55.0	24.6	-34.9
	ESSM-X	-3.6	-2.9	-2.3	-1.4	-2.6	-1.0	-1.0	-0.2	-0.1	-2.3
9 (MOX_16%)	Ref. XS	389.5	388.8	377.9	375.1	375.1	379.9	403.5	450.8	600.1	1272.3
	Subgroup	37.7	37.0	39.7	39.2	37.2	33.0	23.0	10.2	-8.0	-16.1
	ESSM	62.4	63.7	69.7	71.2	72.7	74.3	65.4	51.7	20.0	-35.3
	ESSM-X	-3.5	-5.2	-3.8	-3.6	-2.8	-1.4	-1.5	-0.3	-0.4	-2.4

The MCNP reference cross sections are shown in barns and the entries for the other methods are the relative errors in %. The ring number is ordered from fuel inside to outside.

Table 3 Comparison of spatially dependent U-235 absorption cross sections for Group 22 (116.0eV-117.5eV) with MCNP showing effect of resonance interference

Case		Ring number									
		1	2	3	4	5	6	7	8	9	10
1 (UO2_600K)	Ref. XS	42.3	42.0	41.6	41.2	40.7	40.0	39.2	37.9	36.1	32.6
	Subgroup	-49.2	-48.9	-48.5	-48.0	-47.3	-46.4	-45.3	-43.4	-40.5	-33.9
	ESSM	-49.3	-49.0	-48.5	-48.0	-47.3	-46.4	-45.3	-43.4	-40.5	-34.2
	ESSM-X	-0.1	-0.1	0.0	0.0	0.0	0.0	-0.2	-0.3	-0.9	-2.0
2 (UO2_900K)	Ref. XS	41.5	41.3	40.9	40.4	39.8	39.2	38.2	36.7	34.5	30.9
	Subgroup	-46.8	-46.5	-46.0	-45.3	-44.6	-43.8	-42.3	-40.0	-36.2	-28.4
	ESSM	-46.9	-46.6	-46.1	-45.4	-44.7	-43.8	-42.2	-39.9	-36.1	-28.6
	ESSM-X	-0.5	-0.5	-0.3	-0.1	-0.1	-0.4	-0.4	-0.5	-0.7	-1.5
3 (UO2_1200K)	Ref. XS	38.5	38.4	38.3	37.9	37.4	36.7	35.8	34.3	32.3	29.1
	Subgroup	-41.1	-41.0	-40.9	-40.4	-39.5	-38.6	-36.9	-34.3	-30.1	-22.3
	ESSM	-41.3	-41.2	-41.1	-40.5	-39.6	-38.5	-36.8	-34.1	-29.9	-22.3
	ESSM-X	0.5	0.3	-0.1	0.1	0.2	0.0	0.0	0.0	0.0	-0.7
4 (UO2_para900K)	Ref. XS	39.4	39.5	39.6	39.6	39.4	39.0	38.1	36.9	35.0	31.4
	Subgroup	-42.5	-43.1	-43.5	-43.8	-43.8	-43.6	-42.6	-41.1	-38.1	-31.1
	ESSM	-42.8	-43.2	-43.6	-43.9	-43.8	-43.5	-42.5	-41.0	-38.1	-31.4
	ESSM-X	0.5	0.5	0.4	0.2	0.3	0.1	0.3	0.3	0.1	-0.3
5 (UO2_para1200K)	Ref. XS	36.8	37.1	37.2	37.3	37.1	36.9	36.2	35.1	33.1	29.7
	Subgroup	-36.9	-37.8	-38.5	-39.0	-39.0	-38.9	-38.2	-36.5	-33.0	-25.4
	ESSM	-37.3	-38.1	-38.6	-39.1	-39.0	-38.8	-38.0	-36.3	-32.9	-25.6
	ESSM-X	0.8	0.6	0.7	0.5	0.8	0.5	0.4	0.4	0.6	0.0
6 (UO2_3%)	Ref. XS	42.5	42.1	41.8	41.5	41.0	40.4	39.6	38.3	36.4	32.8
	Subgroup	-49.6	-49.1	-48.8	-48.4	-47.8	-46.9	-45.8	-44.0	-41.0	-34.2
	ESSM	-49.5	-49.0	-48.7	-48.3	-47.7	-46.8	-45.7	-44.0	-41.0	-34.5
	ESSM-X	-0.1	0.1	0.0	-0.2	-0.3	-0.3	-0.6	-0.8	-1.2	-1.9
7 (UO2_4%)	Ref. XS	42.6	42.2	41.9	41.5	41.0	40.4	39.5	38.2	36.3	32.7
	Subgroup	-49.6	-49.1	-48.8	-48.3	-47.7	-46.9	-45.7	-43.8	-40.7	-34.0
	ESSM	-49.6	-49.1	-48.8	-48.3	-47.7	-46.8	-45.6	-43.8	-40.8	-34.3
	ESSM-X	-0.5	-0.3	-0.4	-0.4	-0.5	-0.6	-0.7	-0.7	-1.1	-1.9
8 (UO2_Gd)	Ref. XS	41.7	41.6	41.2	40.9	40.3	39.7	38.8	37.6	35.7	32.4
	Subgroup	-48.7	-48.6	-48.0	-47.5	-46.8	-45.9	-44.7	-42.8	-39.7	-33.5
	ESSM	-48.5	-48.4	-47.8	-47.4	-46.7	-45.8	-44.6	-42.8	-39.8	-33.7
	ESSM-X	0.1	-0.5	-0.2	-0.4	-0.4	-0.5	-0.5	-0.9	-1.1	-2.2
9 (MOX_16%)	Ref. XS	41.1	40.7	40.3	39.9	39.3	38.6	37.6	36.4	34.5	31.3
	Subgroup	-48.6	-47.9	-47.0	-46.3	-45.4	-44.4	-43.0	-40.7	-36.8	-29.7
	ESSM	-47.6	-47.1	-46.5	-46.0	-45.2	-44.2	-42.7	-40.8	-37.6	-31.3
	ESSM-X	-0.4	-0.4	-0.1	-0.3	-0.2	-0.3	-0.3	-0.6	-1.0	-1.9

The MCNP reference cross sections are shown in barns and the entries for the other methods are the relative errors in %. The ring number is ordered from fuel inside to outside.

Multiplying the effective cross sections by group-wise fluxes gives the reaction rate per atom in different rings of the fuel. In order to rule out the flux discrepancies between MCNP and MPACT that are not due to the resonance calculation, instead of directly using the MCNP reaction rates as the reference solution, the resonance effective cross sections tallied from MCNP are input to MPACT to calculate the reference reaction rates. Since the cross section data for fast and thermal groups are still taken from 56-group library for reference calculation, the difference between resonance methods and the reference results is only due to the resonance calculation. In the following comparisons, since the reference results from DeCART calculation using MCNP cross sections are already obtained when ESSM-X was tested in DeCART, we do not regenerate the reference results with MPACT, assuming the differences between DeCART (MCNP XS) and MPACT (MCNP XS) are negligible given the same calculation options applied to the two deterministic codes. To discuss the distributed self-shielding and resonance interference effect separately, two types of figures are created. The first type of figure depicts the radially dependent reaction rates for a specific energy group or integrated over the entire resonance energy range (e.g., 0.625eV to 25keV). This type of figure is best for the dominant isotopes such as U-238. The other type plots the energy dependent reaction rates that are spatially integrated over all fuel annuli. This type of figure best illustrates the resonance interference effect among resonance isotopes, especially for the non-dominant resonance isotopes whose spectra are strongly disturbed by the dominant isotopes.

Figures 2-5 show the radially dependent absorption rates of U-238 for a few representative cases, namely, Cases 2, 4, 8 and 9. In these figures, two resonance groups are considered, Group 34 (6.5eV-6.88eV) and Group 22 (116.0eV-117.5eV), as well as a single group over the entire resonance energy range (0.625eV-25keV). The reference reaction rates are plotted on the upper-left graph of each figure and the rest graphs show the relative errors (%) of the three methods with respect to the reference results for Group 34, 22 and the single group over entire resonance energy range. For ESSM, a 15%-25% underestimation of the total resonance absorption rate in the outermost ring is observed for all four cases. As plutonium buildup tends to peak at the fuel surface, this bias could significantly undermine the accuracy of a multi-region depletion calculation. The errors in the reaction rates with the subgroup method are still significant for an individual group, say Group 34, but tend to be smeared out for the single group over the entire resonance range. Of the three methods, ESSM-X produces the best spatial distribution of the reaction rates, with the largest difference of the entire energy range for any of the cases less than 1.3%.

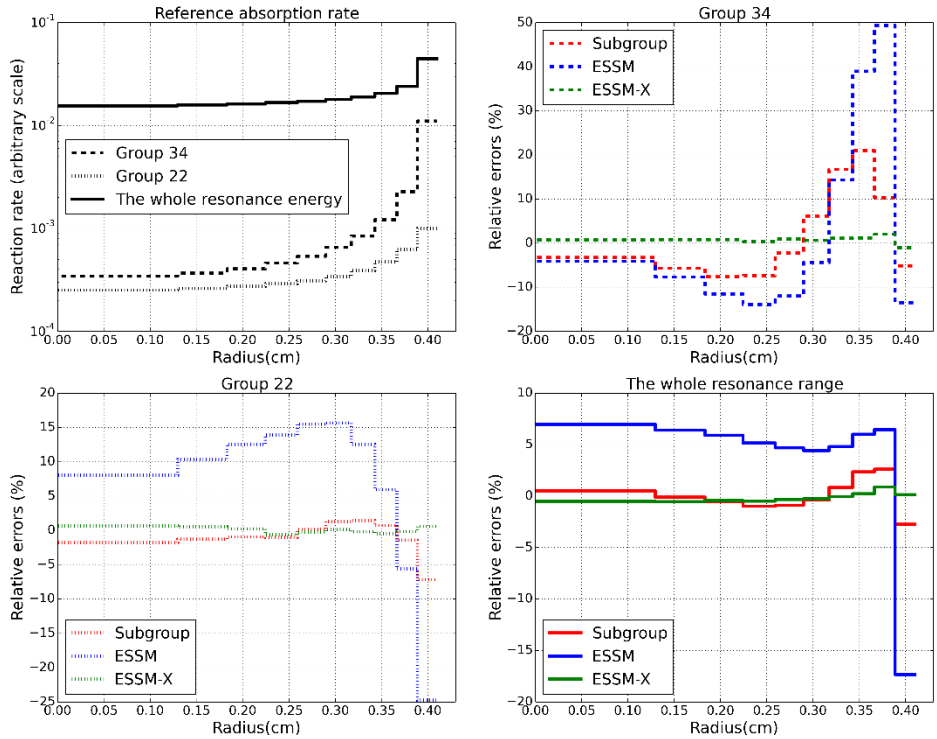

Figure 2 Comparison of radially dependent U-238 absorption rate for Case 2 (UO2_900K)

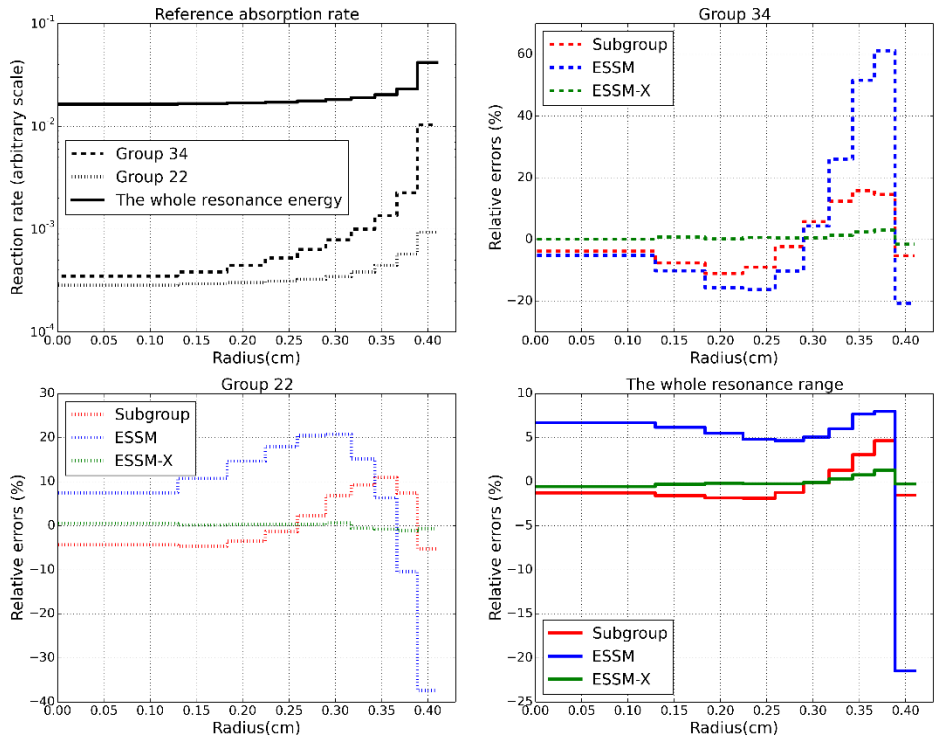

Figure 3 Comparison of radially dependent U-238 absorption rate for Case 4 (UO2_para900K)

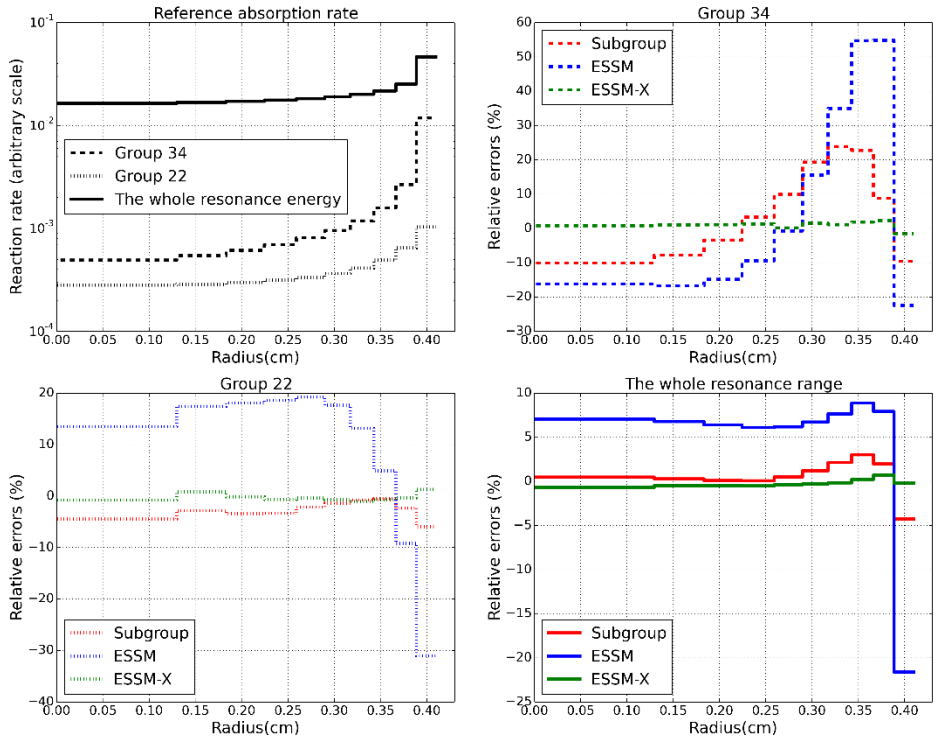

Figure 4 Comparison of radially dependent U-238 absorption rate for Case 8 (UO2_Gd)

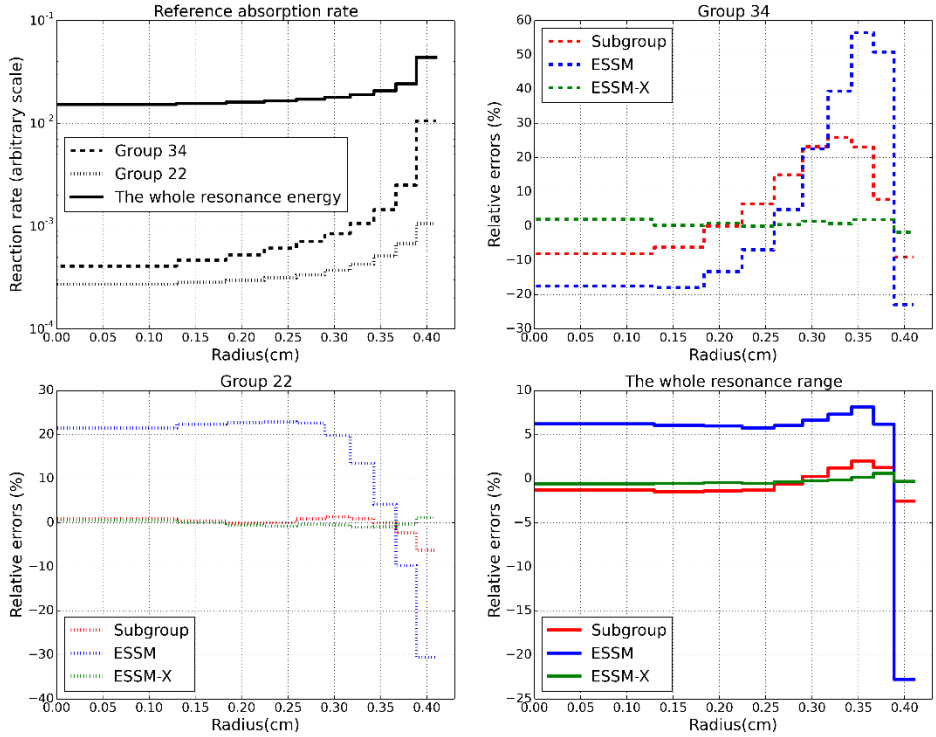

Figure 5 Comparison of radially dependent U-238 absorption rate for Case 9 (MOX_16%)

Next, the resonance interference effect is investigated by comparing the energy dependent reaction rates of the three resonance methods with the reference solution. In Figures 6-10, the reaction rates of major resonance isotopes for Cases 1, 8 and 9 are compared. On the upper side of each figure the reference effective cross section is shown to indicate the importance of energy groups where large reaction rate errors occur. On the lower side shows the relative errors of corresponding reaction rates using three resonance methods with respect to the reference results. Take Figure 6 for example. Both ESSM and the subgroup method treat resonance interference by Bondarenko iteration, which is unable to produce the correct reaction rates for U-235 at the energy ranges where there are large resonances of U-238 (e.g., 6.67eV, 21eV and so on). Since the overlap of the resonances between U-235 and U-238 varies in different energy ranges, the errors of ESSM and the subgroup method can be positive or negative. For all the test cases, ESSM-X significantly improves the energy dependent reaction rates of major resonance isotopes. The resonances of different resonance isotopes interact with each other, resulting in greater relative errors on the isotopes with small densities. In addition to U-235, the absorption rates of Gadolinium isotopes in Case 8 and Plutonium isotopes in Case 9 are all improved by rigorously treating the resonance interference by ESSM-X.

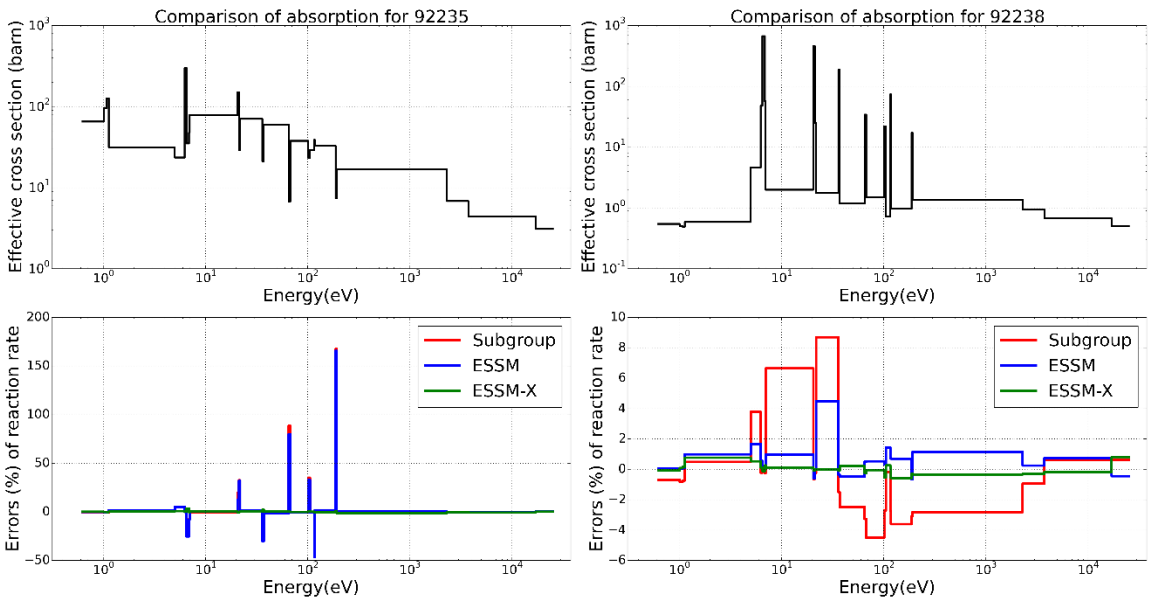

Figure 6 Comparison of energy dependent absorption rate of U-235 and U-238 for Case 1 (UO2-600K)

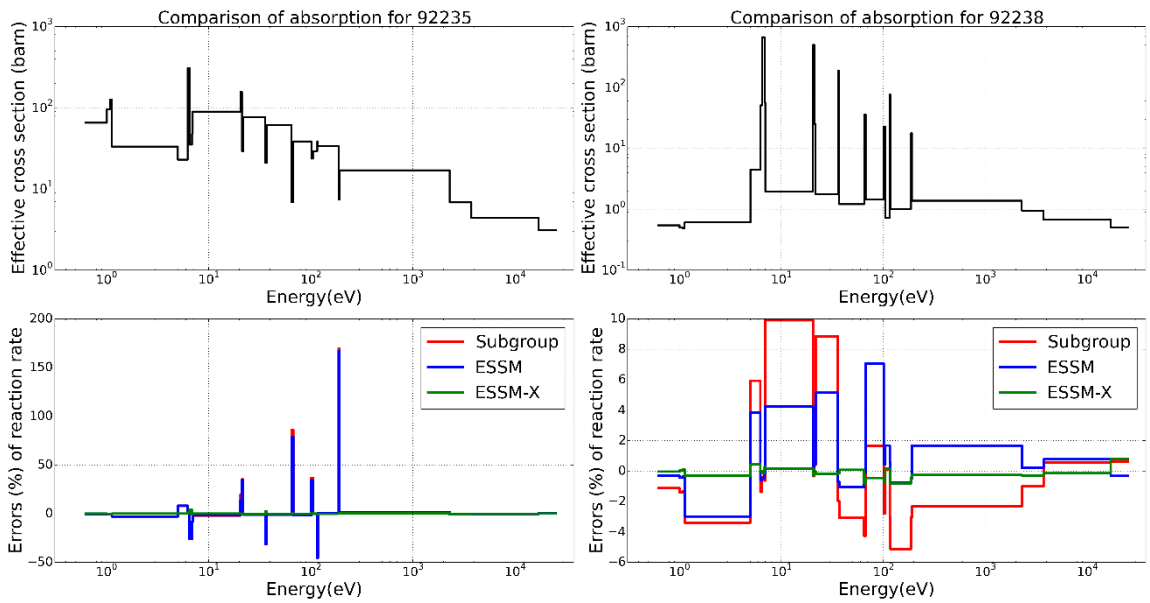

Figure 7 Comparison of energy dependent absorption rate of U-235 and U-238 for Case 8 (UO2-Gd)

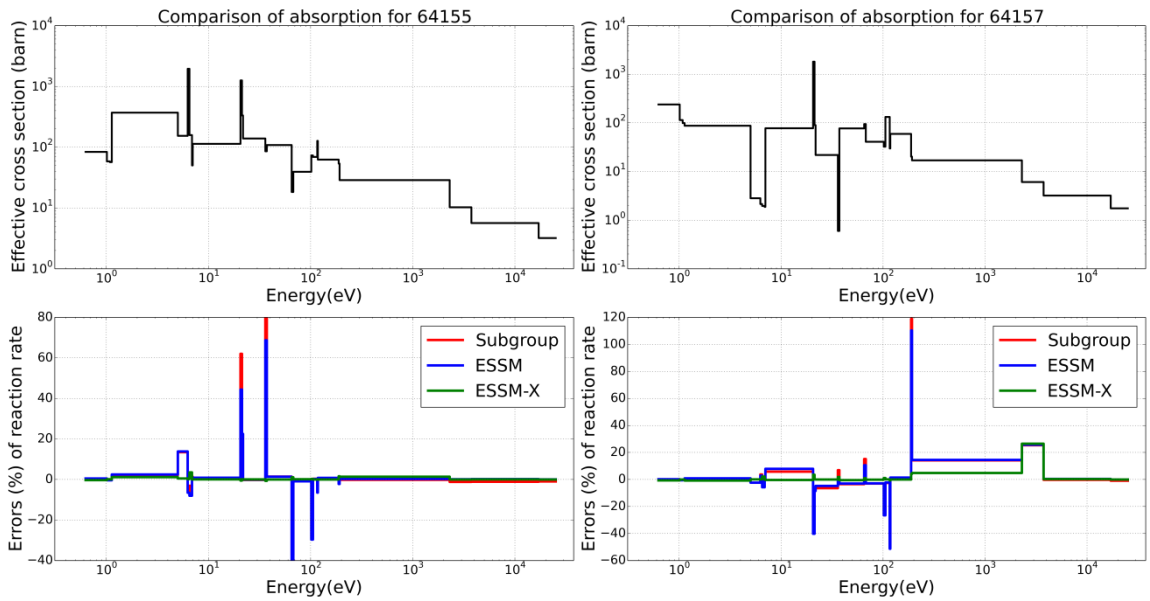

Figure 8 Comparison of energy dependent absorption rate of Gd-155 and Gd-157 for Case 8 (UO2-Gd)

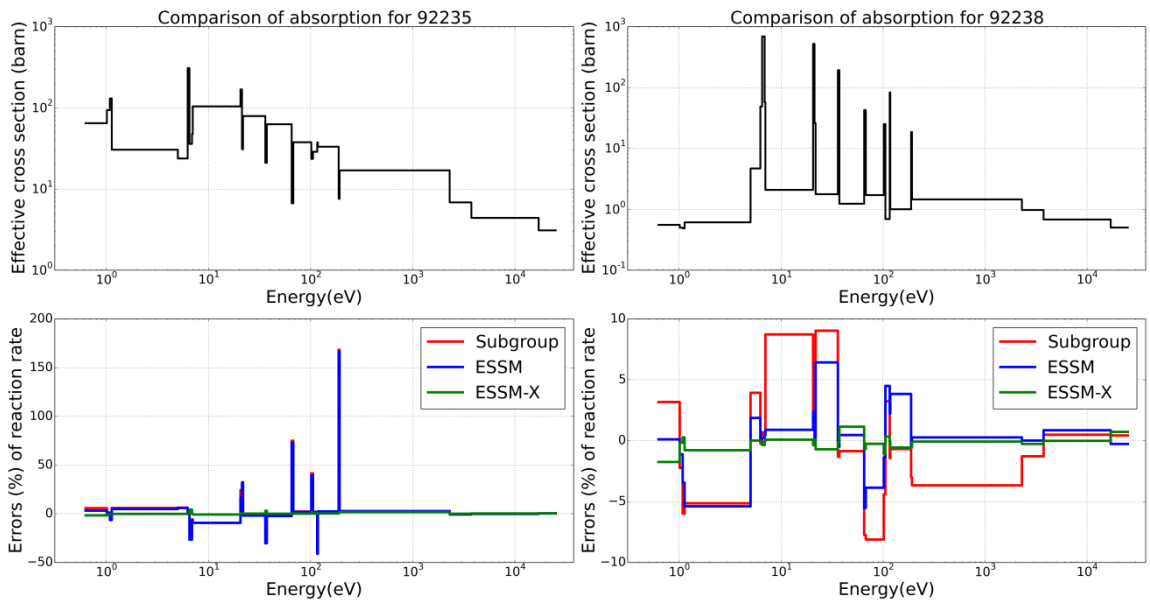

Figure 9 Comparison of energy dependent absorption rate of U-235 and U-238 for Case 9 (MOX-16%)

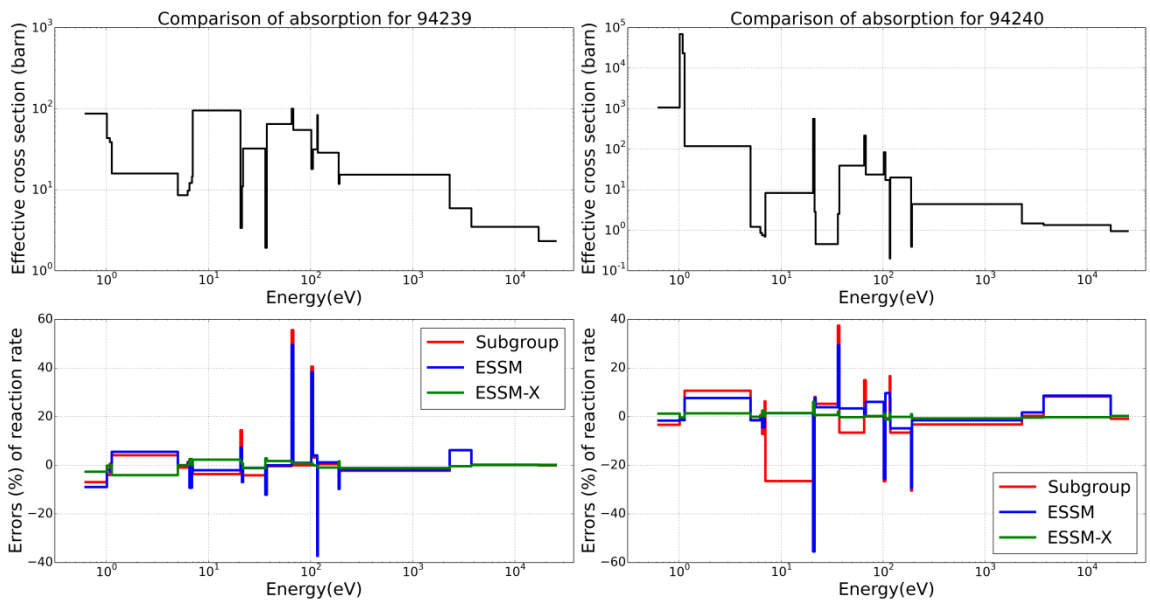

Figure 10 Comparison of energy dependent absorption rate of Pu-239 and Pu-240 for Case 9 (MOX-16%)

Table 4 compares the effective multiplication factors. It has been mentioned in Section 2 that the RI tables used in ESSM-X are generated from UM developed slowing-down solver so that consistency is not guaranteed when the results are compared with the subgroup method and ESSM that employ the cross section data directly from the ORNL 56-group library. Therefore, conclusions are not drawn about how much the eigenvalue could be improved by using ESSM-X, especially for its explicit resonance interference treatment. However, in Cases 8 and 9 where the resonance interference effect becomes severe due to the increased number of resonance isotopes, ESSM-X substantially reduces the error of eigenvalue, indicating the effectiveness of quasi-1D slowing-down model in treating the complex material compositions.

Table 4 Comparison of effective multiplication factors

Case	Ref. k_{eff}	Relative Errors ($\Delta\rho$ in pcm)		
		Subgroup	ESSM	ESSM-X
1	1.39274	-63	29	25
2	1.37980	-70	22	23
3	1.36873	-76	17	22
4	1.38067	-97	45	1
5	1.36956	-101	25	-43
6	1.30346	-24	68	60
7	1.35644	-48	42	38
8	0.22695	-1989	-2185	-214
9	1.21058	-205	-221	-14

As the CE slowing-down calculation is involved in the ESSM-X correction model, it is important to consider the computing resources required for the method. Table 5 compares the computing time and memory usage for the subgroup method, ESSM and ESSM-X, leading to the following observations.

(1) The computing times for ESSM and the subgroup method are primarily determined by the number of fixed source problems to be solved. The average number of iterations to converge equivalence cross sections for each group in ESSM is in the range three to five, which is about the same as the number of subgroup levels. However, the subgroup method distributes the resonance isotopes into resonance categories for the fixed source calculations, which leads to additional computing time for the subgroup method.

(2) Although ESSM-X costs an additional computing time for solving the quasi-1D slowing-down equation, the resonance calculation time T_{res} of ESSM-X is not always greater than ESSM because ESSM-X only converges the equivalence cross section for a single fuel region during the global Dancoff iteration step. Longer T_{res} for ESSM-X are observed for the cases of non-uniform temperature and complex material compositions. This is mainly due to the increased size of the energy mesh for the slowing-down calculation to treat either a large number of nuclides or nuclides

with a number of temperatures involved in the problem. For the cases with complex materials (Cases 8 and 9), the number of resonance isotopes is 3~4 times that of fresh UO_2 fuel, so looping over isotopes to determine the scattering source also becomes more time-consuming. In all, compared to ESSM, ESSM-X increases the total computing time slightly. For a few cases, ESSM-X is even faster than ESSM.

(3) The memory demand of the slowing-down calculation depends primarily on the number of isotopes and the range of temperatures in the problem. It is worth pointing out that the memory used for the slowing-down calculation will not increase with the geometrical size of the problem because the slowing-down calculations for the fuel pins are independent. It primarily depends on the number of isotopes in the fuel region that requires the CE cross section data.

Table 5 Computing resources of the resonance methods

Case	Subgroup			ESSM			ESSM-X		
	T_{tot}[1]	T_{res}[2]	Mem.[3]	T_{tot}	T_{res}	Mem.	T_{tot}	T_{res}	Mem.
1	54.8	28.1	38.5	34.2	7.6	38.5	33.4	6.5	72.5
2	54.3	27.4	38.5	33.8	7.4	38.5	32.8	6.3	72.4
3	54.4	27.2	38.5	34.0	7.3	38.5	33.0	6.4	72.2
4	54.5	27.4	38.5	34.1	7.1	38.5	36.5	9.7	74.6
5	54.3	27.4	38.5	34.3	7.3	38.5	35.9	9.3	74.1
6	54.4	27.5	38.5	34.2	7.3	38.5	33.4	6.6	72.5
7	54.3	27.4	38.5	33.9	7.2	38.5	33.2	6.7	72.5
8	66.0	36.8	38.5	35.9	7.7	38.5	36.6	8.3	99.0
9	70.7	27.7	38.5	48.7	8.9	38.5	49.8	8.8	104.2

[1] T_{tot} is the total computation time (s) of the eigenvalue problem including everything.
[2] T_{res} is the time (s) spent on resonance calculation.
[3] Mem. is the memory usage (MB) of the method.

4. Conclusion

The new resonance self-shielding kernel ESSM-X has been successfully implemented in MPACT. Numerical results show that ESSM-X is capable of resolving the spatially dependent self-shielding of fuel annuli with non-uniform temperature distribution. The error in the U-238 absorption rate over the resonance energy range for the outermost ring is reduced from 15%-25% (ESSM) and 3%-5% (subgroup) to less than 1% (ESSM-X). In addition, the energy dependent reaction rates of non-dominant isotopes such as U-235, Pu-239, Pu-240 are greatly improved by accounting for the resonance interference explicitly.

The computational time of ESSM-X is slightly larger than ESSM for the cases with complex material composition or non-uniform temperature distribution. The memory demand of the slowing-down calculation depends primarily on the number of isotopes and the range of temperatures in the problem. Since the slowing-down calculations for the fuel pins are independent, the memory requirement of the model does not increase with the geometrical size of the problem.

The efficiency of quasi-1D slowing-down kernel would be further improved, for example, by combining the isotopes with similar atomic weights in evaluating the scattering source. The energy mesh thinning scheme might also be improved when a problem has large number of different materials. However, the crucial task at present is to incorporate the quasi-1D kernel into the generation of multigroup cross section data so that a consistent library can be achieved among the subgroup method, ESSM and ESSM-X.

Reference

[1] Y. Liu, W. R. Martin, M. L. Williams and K. S. Kim, "A Full Core Resonance Self-shielding Method Using a Continuous Energy Quasi-1D Slowing-down Solution that Accounts for Temperature-dependent Fuel Subregions and Resonance Interference," (accepted for publication in Nuclear Science and Engineering, 2015).

[2] I. Carlvik, "A Method for Calculating Collision Probabilities in General Cylindrical Geometry and Applications to Flux Distributions and Dancoff Factors," *Proc. Int. Conf. Peaceful Uses of Atomic Energy in Geneva*, **2**, 225, United Nations, New York (1965).

[3] M. L. Williams and M. Asgari, "Computation of Continuous-Energy Neutron Spectra with Discrete Ordinates Transport Theory," *Nucl. Sci. Eng.*, **121**, 173 (1995).

[4] A. Godfrey, "VERA Core Physics Benchmark Progression Problem Specifications," CASL-U-2012-0131-002 (2014).

[5] C. A. Wemple, R. J. J. Stamm'ler and A. A. Ferri, "Improved Temperature-Dependent Resonance Treatment in HELIOS-1.9," *Trans. Am. Nucl. Soc.*, **96**, 657 (2007).